DOI: 10.24874/ti.2048.10.25.12

Tribology in Industry

www.tribology.rs

RESEARCH

Finite Element Analysis on Abrasive Wear Behavior of SKD 11 Tool Steel with Ti and Cr Based Hard Coatings: Material Selections

Riki Hendra Purba[a,*], Deva Ihsan Khoirunas[a], Kenta Kusumoto[b]

[a]*Universitas Pembangunan Nasional Veteran Jakarta, Indonesia,*
[b]*Muroran Institute of Technology, Japan.*

Keywords:

Abrasive wear
Coating
SKD11
TiN
TiAlN
AlCrN
CrN

* Corresponding author:

Riki Hendra Purba
E-mail: Rikihendrapurba@upnvj.ac.id

Received: 18 October 2025
Revised: 19 November 2025
Accepted: 22 December 2025

A B S T R A C T

Abrasive wear remains a critical challenge in tooling and manufacturing processes, as it leads to accelerated material loss, reduced component life, and increased operational costs. This complex phenomenon is governed by dynamic contact conditions, plastic deformation, fracture, and the properties of both the material and interacting abrasive particles. This study uses finite element analysis (FEA) to investigate abrasive wear behavior of JIS SKD11 tool steel coated with Ti- and Cr-based hard coatings, including TiN, TiAlN, CrN, and AlCrN. A single-asperity scratch model was developed to simulate the ploughing wear mechanism, incorporating strain-rate sensitivity via a modified Johnson-Cook model. The simulation results, validated against experimental data, showed good agreement in surface profiles. Wear performance was assessed using degree of wear (β) and degree of penetration (Dp). TiN exhibited the lowest penetration and highest plastic deformation, indicating strong wear resistance. CrN offered the best substrate protection, while AlCrN showed the highest material loss due to brittle failure. Overall, the findings highlight the critical role of coating selection in improving abrasive durability and demonstrate the potential of advanced FEA-based approaches for optimizing protective coatings in tool steel applications.

1. INTRODUCTION

Abrasive wear is a complex phenomenon influenced by dynamic contact conditions, large plastic strains, and fracture, and is further complicated by parameters such as material properties, applied loads, relative humidity, and especially the characteristics of third-body abrasive particles - namely their size, shape, and hardness [1].

Machinery is highly vulnerable to abrasive wear caused by infiltrating hard particles. These contaminants are typically harder than metal components and small enough to bypass filters, allowing them to get trapped between moving surfaces. Once caught, they grind away at the machine parts, causing rapid wear. This damage leads directly to reduced performance, more

frequent servicing, and a greater likelihood of total equipment failure [2-4]. Wear of machinery parts and tooling significantly affects productivity, efficiency, reliability, and the quality of manufactured equipment and products. It has long been a critical concern due to its impact on tool life, the need for frequent component repairs, equipment failures, and costly production line interruptions. As industrial trends move toward higher production speeds and the use of lighter materials, the velocity and stress levels experienced by machinery and tools are expected to rise, intensifying wear-related issues. For this reason, studying the abrasive wear process is critical for creating solutions to prevent these outcomes [4,5].

Tool steels such as JIS SKD11, also designated as AISI D2, are a prevalent material choice for applications in the metal forming, die manufacturing, and cutting tool industries. The widespread utilization of SKD11 in these sectors is attributable to its desirable mechanical properties, notably high hardness, high compressive strength, and excellent wear resistance. Its specific properties make this steel highly suitable for the fabrication of tooling and mechanical parts, notably for applications like extrusion molds, plastic injection molds, and dies for pressure casting [6-10].

The use of coatings on material surfaces has become one of the most effective methods for improving a material's resistance to wear. Coatings can increase material hardness at high temperatures and provide a chemical barrier to reduce diffusion or reactions between the material and the workpiece, thereby minimizing wear on the material [11-13].

Coatings based on Titanium and Chromium nitrides are commonly utilized for surface protection. As an extension of this, ternary nitride systems—including CrN, TiAlN, TiN, TiCN and AlCrN—have been the subject of numerous investigations focusing on their deposition and resultant properties when applied using various PVD techniques [14]. Various types of coatings have been developed using several deposition processes, one of which is PVD (Physical Vapor Deposition). Over the past few decades, Titanium Nitride (TiN) has been widely used as a coating material for cutting tools, dies, and various machine components. However, TiN as a coating material has limitations in its resistance to oxidation at high temperatures. To address this, aluminum has been added to TiN, forming Titanium Aluminum Nitride (TiAlN), to enhance the coating's resistance to high temperatures. The addition of aluminum also increases the coating's hardness and improves its corrosion resistance [15-20].

Numerical and experimental approaches have been widely employed to investigate abrasive wear mechanisms, particularly through single-asperity scratch testing. Wechsuwanmanee et al. [21] developed a finite element (FE) model based on their experimental scratch tests and demonstrated that the simulation could replicate the overall experimental trends, though noticeable discrepancies remained, indicating the need for refinement in modelling strategies. Similarly, Pondicherry et al. [22] proposed a load-controlled single-asperity scratch simulation for martensitic steel and reported good agreement between predicted and experimental scratch depths. Deviations observed at loads above 10 N were attributed to the absence of a material damage model in their formulation.

Woldman et al. [3] experimentally examined the influence of abrasive body dimensions by varying indenter radii (50, 100, and 200 μm), concluding that smaller indenters generate higher wear rates at constant load due to increased groove volume. Similar behaviour was previously reported by Masen et al. [23], who observed the same dependency in their study of abrasive wear on nodular cast iron. In subsequent study, Woldman et al. [2] investigated abrasive wear behavior using Finite Element Analysis (FEA) and a single-asperity scratch test. It was found that the FEA method can accurately model the ploughing abrasive mechanism, as shown by the surface profile, which closely matches the experimental results. However, the simulation could not fully replicate the wedge and cutting mechanisms because they occur under transient conditions. Mac et. al [24] proposes an improved method for predicting cutting force (F) and chip shrinkage coefficient (K) during the milling of SKD11 alloy steel by combining experiments and FEM simulations. Initial predictions using the Johnson–Cook fracture model showed large deviations, leading to the development of a modified fracture model based on the relationship between equivalent strain and stress triaxiality. Incorporating experimental data, the

new model significantly reduced prediction errors, with maximum deviations of 5.29% for F and 5.08% for K. The method offers a more accurate and efficient approach for simulating and optimizing machining of SKD11 steel.

Research on coated systems further illustrates the complexity of tribological behaviour. Yoon et al. [16] experimentally compared TiN and TiAlN coatings deposited on AISI D2 steel using arc ion plating. They observed that adhesive wear dominated during sliding against a steel ball, whereas abrasive wear was dominant against an alumina counter body. The friction coefficient decreased with increasing sliding speed for steel–coating contact but increased when sliding against alumina. At high sliding speeds, TiAlN exhibited a lower friction coefficient than TiN, indicating its suitability for high-speed machining.

Previous numerical studies of single asperity scratch tests have largely been restricted to analysing abrasive wear in uncoated monolithic materials. Research on abrasive wear in coated systems, however, has predominantly relied on experimental methods, and comprehensive numerical modelling in this area remains limited. To address this gap, the present work develops an enhanced single-asperity abrasion model for coated substrates by building upon and extending established simulation frameworks. This approach enables a more detailed investigation of the abrasive wear mechanisms in PVD coated materials and facilitates the identification of coating materials with superior abrasion resistance.

2. METHODOLOGY

This study follows the structured research methodology illustrated in Fig. 1. The process begins with a literature review to establish a theoretical foundation, followed by a pre-processing stage where the finite element model is defined, including its mesh, boundary conditions, and material properties. The model is then solved using the Finite Element Method. In the post-processing phase, simulation data is extracted and analyzed. A critical validation step compares these results against experimental or theoretical data. This workflow incorporates an iterative loop, returning to the pre-processing stage if results are invalid, to ensure the final analysis is based on robust and validated data.

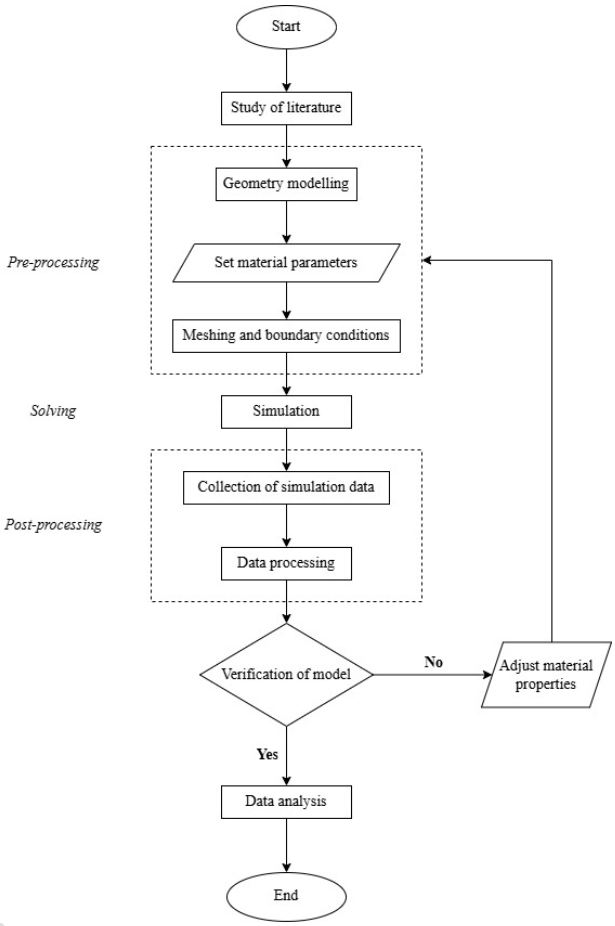

Fig. 1. Research flowchart.

2.1 Model and mesh

To simulate the abrasive wear process, a finite element model was developed in Ansys LS-Dyna using an explicit dynamics solver to accurately capture plastic deformation and material removal. The modelling framework adopted in this study is based on the single-asperity abrasion model proposed by Woldman et al. [2], with several modifications. The primary enhancement is the introduction of a 10 μm-thick coating layer on top of the substrate. As shown in Fig. 2a, the specimen dimensions are 300 × 200 × 30 μm, comprising a 20 μm-thick substrate and a 10 μm coating layer. The indenter is idealized as a spherical body with a radius of 50 μm to reduce computational cost. It is modelled as a rigid, non-deformable sphere and fully constrained in all degrees of freedom. The interface between the coating and substrate is defined as perfectly bonded. Automatic Surface to Surface contact is used to define the contact between the coating and the indentor. The specimen is constrained in the y and z directions, while

abrasive motion is generated by fixing the indenter and applying a prescribed displacement to the specimen along the x-axis (Fig. 2b). The mesh is refined near the contact region, with element sizes of 1 μm for the coating, 2 μm for the substrate, and 3 μm for the indentor.

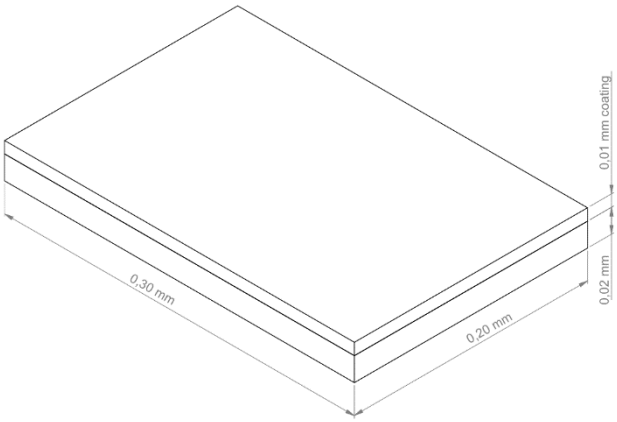

(a) Specimen geometry

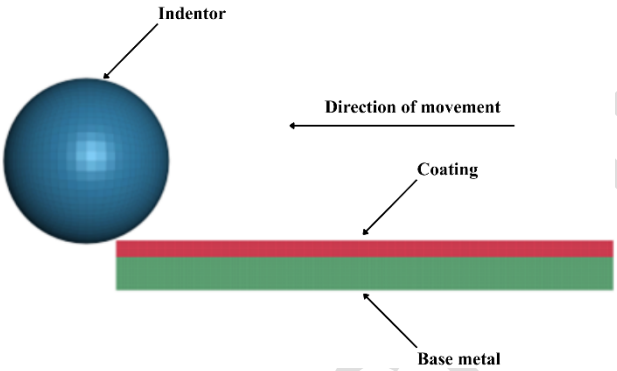

(b) Simulation model

Fig. 2. Simulation geometry.

2.2 Material properties

This study builds upon the methodology established in previous research, which utilized a rigid SiO_2 indenter interacting with an St 52 steel substrate. In the present work, the model is adapted to represent a coated system comprising a JIS SKD11 tool steel substrate and four distinct coating materials.

The SKD11 substrate was described by a modified Johnson–Cook (JC) constitutive model, which accounts for strain hardening, strain-rate sensitivity, and thermal softening, while also including a failure criterion to represent ductile fracture under high strain-rate conditions. Flow stress was expressed in equation (1) below [25].

This model calculates the von Mises equivalent true stress (σ) as a function of equivalent plastic strain (ε_{pl}), plastic strain rate ($\dot{\varepsilon}$), and a normalized temperature (T* or T_{norm}). The relationship, shown in Equation (1), is composed of three terms representing plastic strain hardening, strain-rate hardening, and thermal softening. The normalized temperature (T*), defined in Equation (2), is calculated by dividing the difference between the operating temperature (T) and a reference temperature (T_{ref}) by the difference between the material's melting temperature (T_m) and the same reference temperature.

The model calculates the equivalent fracture strain (ε_f) as a function of stress triaxiality (σ^*), the plastic-to-reference strain rate ratio (ε_{pl} / ε_0), and the relationship between the current temperature (T), melting temperature (T_m), and reference temperature (T_r) temperatures as shown in equation (3). This relationship is defined by five material constants (D1 to D5), which were determined experimentally. The first three constants, D1, D2, and D3, were obtained by fitting fracture strain curves from tensile tests on various specimen geometries to capture the effect of stress triaxiality. The final two constants, D4 and D5, were derived by analyzing the specific influence of strain rate and temperature on fracture strain, respectively [10].

The SiO_2 particle was modeled as a rigid body to ensure that no deformation occurred during the simulation. In contrast, the TiAlN coating was represented using a general plastic-kinematic material model, owing to the limited availability of detailed mechanical property data for this coating material. The mechanical properties employed in the simulation are summarized in Table 1.

$$\sigma = (A + B\varepsilon_{pl}^{n})\left(1 + C\ ln\left\{\frac{\dot{\varepsilon}}{\dot{\varepsilon}_{ref}}\right\}\right)(1 - T_{norm}^{m}) \quad (1)$$

$$T_{norm}\ or\ T^* = (T - T_{ref})/(T_m - T_{ref}) \quad (2)$$

$$\varepsilon_f = [D_1 + D_2 \exp(D_3\sigma^*)]\left[1 + D_4 \ln\left(\frac{\dot{\varepsilon}^{pl}}{\dot{\varepsilon}_0}\right)\right]\left[1 + D_5\left(\frac{T - T_r}{T_m - T_r}\right)^{m}\right] \quad (3)$$

Table 1. Material properties [2,6,26-37].

Material	Density (Kg/m³)	Hardness (GPa)	Young's modulus (GPa)	Poisson Ratio
ST-52	7800	2	210	0.3
SKD 11	8400	7	210	0.3
SiO2	2200	9.8	73	0.17
TiN Coating	5400	26	290	0.25
TiAlN Coating	5200	30	492.5	0.25
AlCrN Coating	5200	31	600	0.3
CrN Coating	5900	18	240	0.25

2.3 Wear Mechanisms

A single-asperity scratch test produces a groove on a specimen's surface as shown in Fig. 3a, with the cross section illustrated in Fig. 3b. There are three primary abrasive mechanisms: ploughing, cutting, or wedge formation. The dominant mechanism is dictated by factors such as the degree of penetration (a function of applied load) and the interfacial shear strength. At low penetration depths, ploughing occurs, where material is plastically displaced to form shoulders alongside the groove with no significant material loss. Cutting, the most severe mechanism, involves the removal of material as a chip and is typically observed only under high loads with sharp particles. Finally, wedge formation is a non-steady-state process where displaced material accumulates into a bow ahead of the tip, which cyclically grows and detaches as a wear particle [2,38,39].

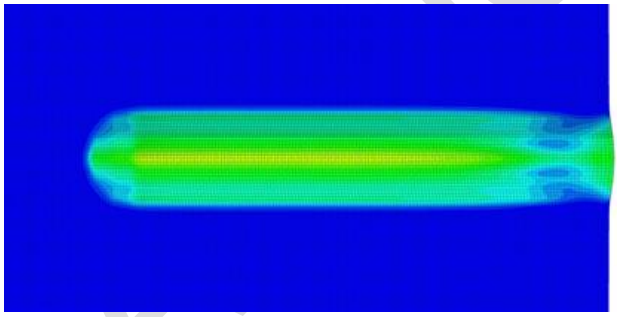

(a) Schematic illustration of the cross section of a wear scar

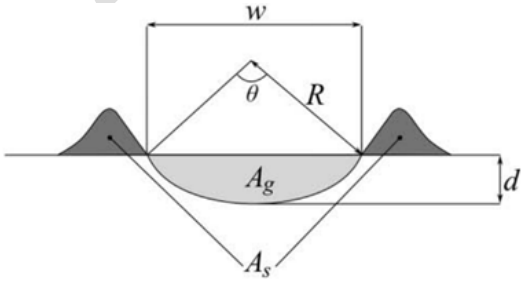

(b) Resulting groove from simulation [2]

Fig. 3. Resulting groove from scratch test.

The wear produced by the scratching process can be quantified using the degree of wear parameter, which expresses the fraction of displaced material that is permanently removed from the surface. An idealized cross-sectional representation of the resulting wear scar is shown in Fig. 3b, where A_g denotes the groove area, A_s the shoulder area, w the groove width, and d the indentation depth. Multiplying A_g and A_s by the scratch length l yields the corresponding groove and shoulder volumes, V_g and A_s, respectively [3]. The net volume of material removed from the surface is therefore given by V_g–V_s. The degree of wear, denoted as β, is defined accordingly in Equation (4) [40],

$$\beta = \frac{V_g - V_s}{V_g} \tag{4}$$

A value of β = 1 corresponds to ideal material removal, where pure cutting occurs without any ploughing, whereas β = 0 represents ideal ploughing with no net material loss. Because the scratch length is identical for all materials examined in this study, the degree of wear expression can be simplified as:

$$\beta = \frac{A_g - A_s}{A_g} \tag{5}$$

Additionally, the degree of penetration (D_p) can be used to assess the severity of contact by quantifying the relative depth of the groove, as defined in Equation (6) [41].

$$D_p = \frac{2d}{w} \tag{6}$$

3. RESULTS AND DISCUSSIONS

3.1 Validation

To ensure the reliability of the simulation model, a validation procedure was performed by reproducing the simulation setup reported by Woldman et al. [2] and comparing the resulting

surface profile with data from their numerical and experimental study. As shown in Fig. 4, the simulated surface profile exhibits close agreement with the reference results, demonstrating that the developed model accurately captures the ploughing wear mechanism. Following validation, the specimen geometry was modified by incorporating a coating layer. The substrate material was replaced with SKD11, using material parameters reported by Wang et al. [37]. The TiAlN coating was modelled using a general plastic–kinematic material formulation due to the limited availability of comprehensive mechanical property data for this coating.

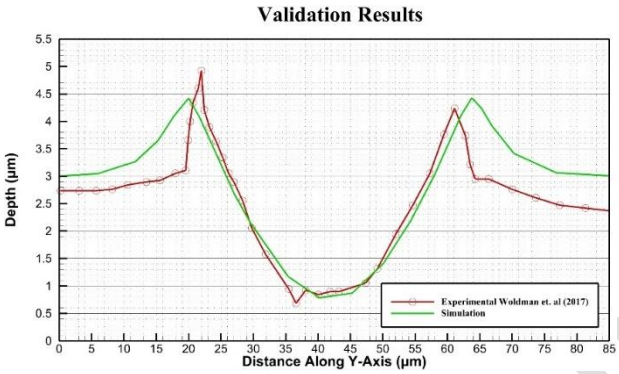

Fig. 4. Validation results.

3.2 Surface profile

Fig. 5 presents the simulated surface profiles of the coated specimens after the scratch test, alongside the baseline uncoated SKD11. As shown in Fig. 5a, all coated specimens exhibit improved resistance to abrasion compared to the uncoated substrate, evident from the reduced groove depth and smaller shoulder formation. Among the coatings, TiN demonstrates the most favourable performance, producing the smallest groove and shoulder areas. This trend is consistent with the equivalent plastic strain results in Fig. 6a, where TiN shows the lowest strain levels. The simulation findings also align with the experimental observations reported by Danisman et al. [42] and Yoon et. al. [16], who found that TiN produced the smallest wear track width, outperforming TiAlN. In contrast, CrN exhibits the largest shoulder area, while AlCrN produces the greatest groove area. Regarding plastic deformation, CrN shows the highest equivalent plastic strain, followed by AlCrN and TiAlN, as illustrated in Fig. 6b, 6c, and 6d, respectively.

Fig. 5b illustrates the surface profiles of the substrate beneath each coating material. The data indicate that the substrate beneath the AlCrN coating exhibits the deepest groove, followed by that under the TiAlN coating. Conversely, the substrate beneath the CrN coating shows the shallowest groove, with the TiN-coated substrate displaying slightly deeper penetration.

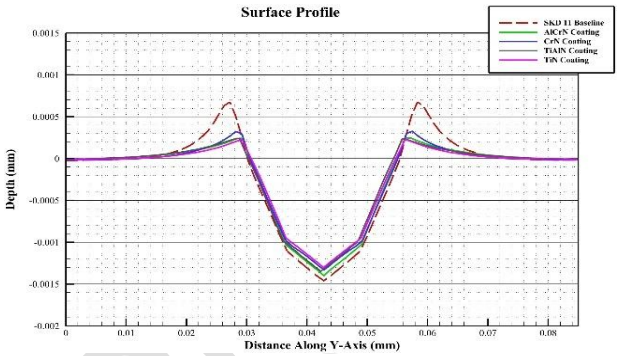

(a) Surface profile of coating material

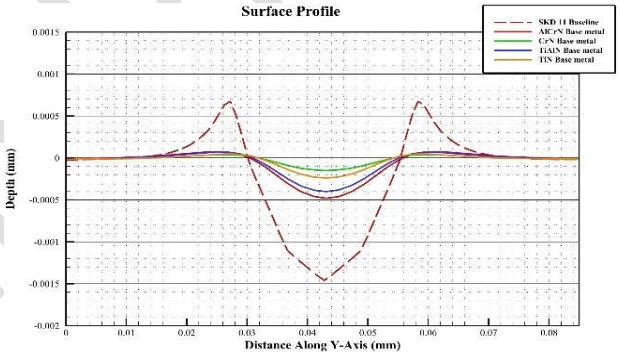

(b) Surface profile of base material

Fig. 5. Resulting surface profile.

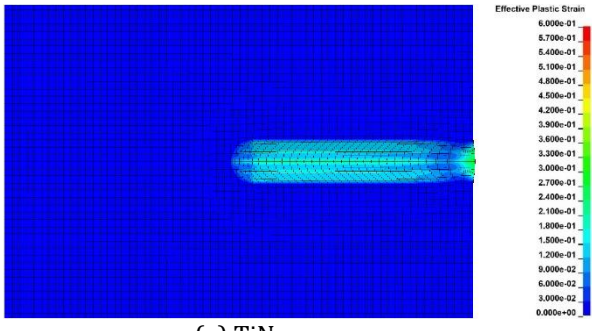

(a) TiN

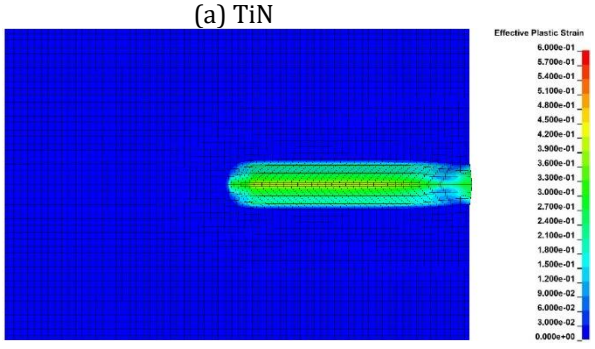

(b) CrN

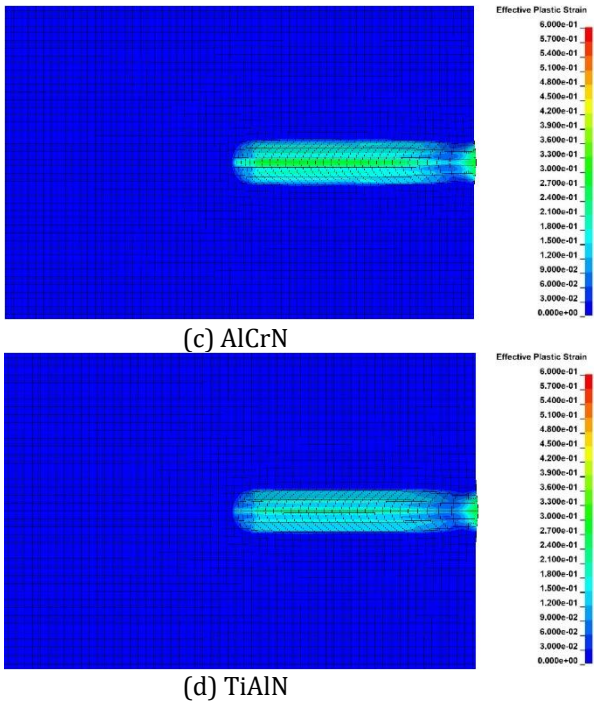

(c) AlCrN

(d) TiAlN

Fig. 6. Wear track of the coating material.

3.3 Coating material wear parameter

The wear parameters for the coating materials, calculated using Equations (2) and (3), are summarized in Table 2. The results indicate that all coated specimens exhibit a higher degree of wear compared to the uncoated SKD11. However, in terms of degree of penetration, both TiN and CrN coatings demonstrate lower values than the uncoated substrate, suggesting better resistance to penetration. Among all coatings, TiN exhibits the highest degree of wear at 0.83858, yet also the lowest degree of penetration at 0.113975, indicating efficient material removal with minimal subsurface damage. TiAlN shows the lowest degree of wear at 0.79751, followed by CrN and AlCrN. The highest degree of penetration, 0.122748, is observed in the AlCrN coating, followed by TiAlN and CrN.

The elevated degree of wear observed across all coatings indicates a stronger tendency toward cutting-dominated wear when material failure is permitted. This trend can be attributed to the reduced shoulder area in the scratch profiles of the coated specimens, which lowers the amount of displaced but unreleased material, thereby increasing the net wear volume relative to the uncoated SKD11 [3].

3.4 Base metal wear parameter

The wear parameters for the substrate beneath each coating material are summarized in Table 3. The results reveal that, with the exception of CrN, all coated substrates exhibit a higher degree of wear compared to the uncoated SKD11. In terms of degree of penetration, however, all coated substrates demonstrate lower values than the uncoated counterpart, indicating improved resistance to subsurface deformation. Among the coatings, CrN provides the most effective protection, with the underlying substrate exhibiting the lowest degree of wear and penetration, measured at 0.623116 and 0.014785, respectively. In contrast, the substrate beneath the AlCrN coating shows the highest degree of wear at 0.755775 and the greatest penetration depth at 0.039139, followed by those under the TiAlN and TiN coatings.

The relatively high degree of wear observed in some coated samples is primarily attributed not to severe material removal, but to the very low degree of penetration. As illustrated in Fig. 5b, the wear depth is extremely small (less than 0.5 μm), indicating that most of the applied load is absorbed by the coating layer. Under such low penetration conditions, the material is more likely to deform downward into the groove rather than laterally into the shoulders. This results in a large groove area and a minimal shoulder area. The significant disparity between groove and shoulder areas artificially increases the calculated degree of wear, despite the actual wear depth being very small [3].

Table 2. Coating material wear parameters.

Coating Material Wear Parameters					
Parameters	**SKD11 Uncoated**	**AlCrN**	**CrN**	**TiAlN**	**TiN**
Degree of wear	0.637010	0.80540	0.79670	0.79751	0.83858
Degree of penetration	0.116331	0.122748	0.115154	0.118220	0.113975

Table 3. Base metal degree of wear.

Base Material Wear Parameters					
	SKD11 Uncoated	**AlCrN**	**CrN**	**TiAlN**	**TiN**
Degree of wear	0.637010	0.788775	0.623116	0.723306	0.712379
Degree of penetration	0.116331	0.039139	0.014785	0.039084	0.025906

3.5 Abraded fraction

To quantify the fraction of abraded material, as illustrated in Fig. 7, a failure criterion was applied to the coating material parameters by specifying their respective failure strain values. The results indicate that the TiN coating exhibits the least material removal over time followed closely by TiAlN. In contrast, the CrN and AlCrN coatings display similar trends, both experiencing the highest levels of material loss. The trends observed for TiN and TiAlN are consistent with the experimental findings reported by Yoon et al. [16], where TiN demonstrated the least wear, followed by TiAlN. Experimentally, the superior wear resistance of TiN is attributed to its fine-grained microstructure, as finer grains generally enhance wear resistance compared to coarser-grained materials [42].

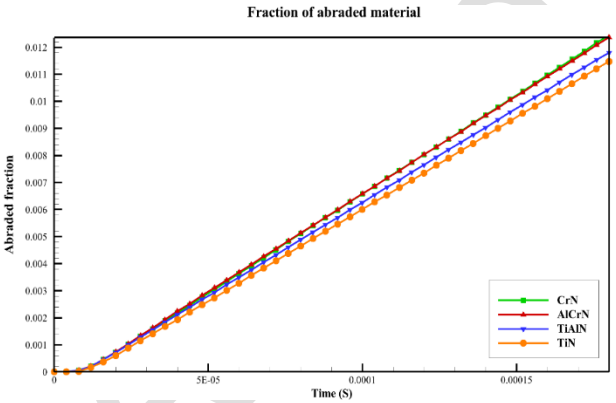

Fig. 7. Fraction of abraded material during the simulation.

As shown in Fig. 8a, TiN undergoes more plastic deformation, which contributes to its lower erosion rate. Similarly, the TiAlN and CrN coatings exhibit limited plastic deformation as shown in Fig. 8b and c respectively, resulting in moderate material removal. In comparison, the AlCrN coating shows no plastic deformation, which corresponds to the highest material loss among the coatings evaluated as shown in Fig. 8d.

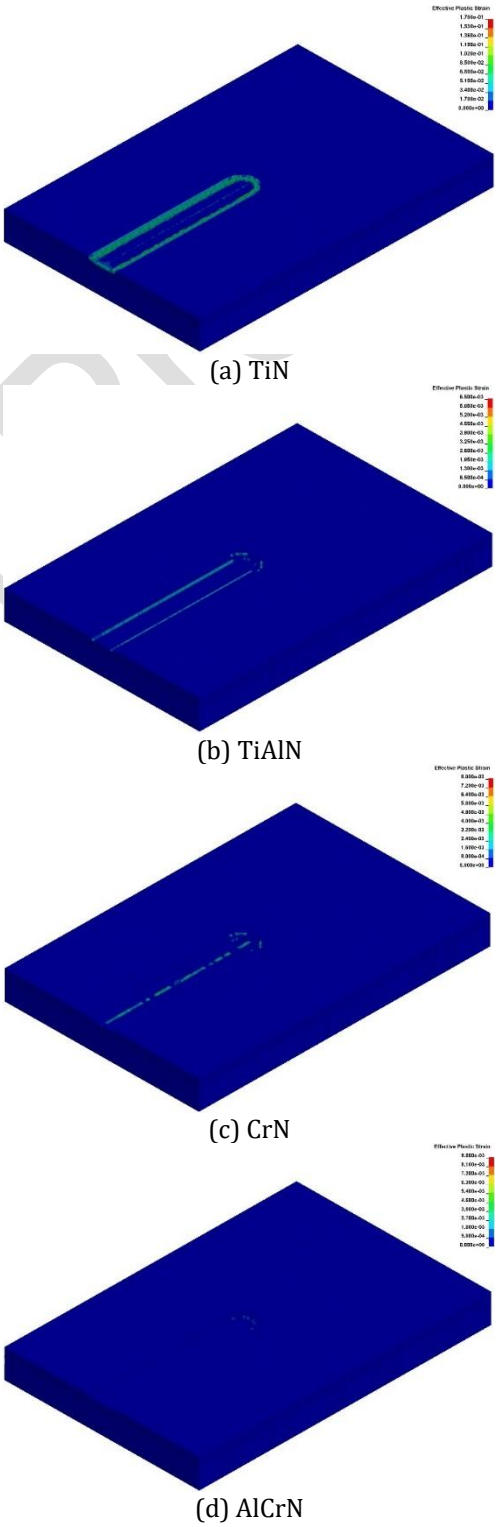

(a) TiN

(b) TiAlN

(c) CrN

(d) AlCrN

Fig. 8. Cutting mechanism on the material surfaces.

4. CONCLUSIONS

This study investigated the abrasive wear behavior of SKD11 tool steel with various Ti- and Cr-based hard coatings using finite element analysis. The results demonstrated that all coatings improved wear resistance compared to the uncoated substrate, with TiN showing the most favorable performance in terms of minimal groove formation, low equivalent plastic strain, and the lowest degree of penetration. TiN exhibited the least material loss, followed by TiAlN, AlCrN, and CrN, consistent with previous experimental findings [16,41]. In contrast, CrN and AlCrN experienced the highest material removal due to their limited capacity for plastic deformation. The elevated degree of wear observed across all coatings suggests a stronger tendency toward cutting-dominated wear once material failure is allowed. This behavior is linked to the reduced shoulder formation in coated specimens, which decreases the volume of displaced but retained material and increases the effective wear volume relative to uncoated SKD11 [3]. These findings underscore the importance of selecting appropriate coating materials to balance hardness, plastic deformation, and failure resistance for improved abrasive wear performance.

In addition, some machine part should experience high temperature abrasive wear in the real application. Therefore, this present study can be developed to predict the wear depth of worn surface corresponding to wear rate where the influence of temperature is involved in investigation [43]. Moreover, this study can be used for further work which is focused other surface modification such as cast insert in method or additively manufactured [44,45].

REFERENCES

[1] M. A. Masen, M. B. De Rooij, D. J. Schipper, K. Adachi, and K. Kato, "Single asperity abrasion of coated nodular cast iron," *Tribology International*, vol. 40, no. 2, pp. 170–179, Apr. 2006, doi: 10.1016/j.triboint.2005.11.023.

[2] M. Woldman, E. Van Der Heide, T. Tinga, and M. A. Masen, "A finite element approach to modeling abrasive wear modes," *Tribology Transactions*, vol. 60, no. 4, pp. 711–718, Jul. 2016, doi: 10.1080/10402004.2016.1206647.

[3] M. Woldman, E. Van Der Heide, T. Tinga, and M. A. Masen, "The influence of abrasive body dimensions on single asperity wear," *Wear*, vol. 301, no. 1–2, pp. 76–81, Dec. 2012, doi: 10.1016/j.wear.2012.12.009.

[4] M. Woldman, E. Van Der Heide, D. J. Schipper, T. Tinga, and M. A. Masen, "Investigating the influence of sand particle properties on abrasive wear behaviour," *Wear*, vol. 294–295, pp. 419–426, Jul. 2012, doi: 10.1016/j.wear.2012.07.017.

[5] J. D. Bressan, R. Hesse, and E. M. Silva, "Abrasive wear behavior of high speed steel and hard metal coated with TiAlN and TiCN," *Wear*, vol. 250, no. 1–12, pp. 561–568, Oct. 2001, doi: 10.1016/s0043-1648(01)00638-x.

[6] J. L. Li, L. L. Jing, and M. Chen, "An FEM study on residual stresses induced by high-speed end-milling of hardened steel SKD11," *Journal of Materials Processing Technology*, vol. 209, no. 9, pp. 4515–4520, Dec. 2008, doi: 10.1016/j.jmatprotec.2008.10.042.

[7] S. Cho, I. Jo, H. Kim, H.-T. Kwon, S.-K. Lee, and S.-B. Lee, "Effect of TiC addition on surface oxidation behavior of SKD11 tool steel composites," *Applied Surface Science*, vol. 415, pp. 155–160, Nov. 2016, doi: 10.1016/j.apsusc.2016.11.164.

[8] S.-H. Chang, C.-C. Yu, K.-T. Huang, and C.-M. Liu, "Deposition of DLC/oxynitriding Films onto JIS SKD11 Steel by Bipolar-pulsed PECVD," *ISIJ International*, vol. 55, no. 12, pp. 2631–2638, Jan. 2015, doi: 10.2355/isijinternational.isijint-2015-350.

[9] M. A. S. B. A. Rahim, M. B. Minhat, N. I. S. B. Hussein, and M. S. B. Salleh, "A comprehensive review on cold work of AISI D2 tool steel," *Metallurgical Research & Technology*, vol. 115, no. 1, p. 104, Nov. 2017, doi: 10.1051/metal/2017048.

[10] T.-B. Mac, T.-T. Luyen, and D.-T. Nguyen, "A Study for Improved Prediction of the Cutting Force and Chip Shrinkage Coefficient during the SKD11 Alloy Steel Milling," *Machines*, vol. 10, no. 4, p. 229, Mar. 2022, doi: 10.3390/machines10040229.

[11] M. H. Staia, M. D'Alessandria, D. T. Quinto, F. Roudet, and M. M. Astort, "High-temperature tribological characterization of commercial TiAlN coatings," *Journal of Physics Condensed Matter*, vol. 18, no. 32, pp. S1727–S1736, Jul. 2006, doi: 10.1088/0953-8984/18/32/s04.

[12] A. Rizzo *et al.*, "Improved properties of TiAlN coatings through the multilayer structure," *Surface and Coatings Technology*, vol. 235, pp. 475–483, Aug. 2013, doi: 10.1016/j.surfcoat.2013.08.006.

[13] J. Deng, F. Wu, Y. Lian, Y. Xing, and S. Li, "Erosion wear of CrN, TiN, CrAlN, and TiAlN PVD nitride coatings," *International Journal of Refractory Metals and Hard Materials*, vol. 35, pp. 10–16, Mar. 2012, doi: 10.1016/j.ijrmhm.2012.03.002.

[14] T. M. Cholakova *et al.*, "Ti- and Cr-based hard coatings obtained at low temperatures by unbalanced magnetron sputtering," *Journal of Physics Conference Series*, vol. 992, p. 012030, Mar. 2018, doi: 10.1088/1742-6596/992/1/012030.

[15] J. M. Castanho and M. T. Vieira, "Effect of ductile layers in mechanical behaviour of TiAlN thin coatings," *Journal of Materials Processing Technology*, vol. 143–144, pp. 352–357, Apr. 2003, doi: 10.1016/s0924-0136(03)00454-0.

[16] S.-Y. Yoon, J.-K. Kim, and K. H. Kim, "A comparative study on tribological behavior of TiN and TiAlN coatings prepared by arc ion plating technique," *Surface and Coatings Technology*, vol. 161, no. 2–3, pp. 237–242, Nov. 2002, doi: 10.1016/s0257-8972(02)00474-7.

[17] T. M. Cholakova *et al.*, "Protective multilayer (Ti, Al) N coatings deposited at low temperature by closed-field unbalanced magnetron sputtering," *Bulgarian Chemical Communications*, vol. 48, pp. 384–390, 2016.

[18] J. C. Oliveira, A. Manaia, and A. Cavaleiro, "Hard amorphous Ti–Al–N coatings deposited by sputtering," *Thin Solid Films*, vol. 516, no. 15, pp. 5032–5038, Feb. 2008, doi: 10.1016/j.tsf.2008.02.006.

[19] W. Münz, "Titanium aluminum nitride films: A new alternative to TiN coatings," *Journal of Vacuum Science & Technology a Vacuum Surfaces and Films*, vol. 4, no. 6, pp. 2717–2725, Nov. 1986, doi: 10.1116/1.573713.

[20] E. Santecchia, A. M. S. Hamouda, F. Musharavati, E. Zalnezhad, M. Cabibbo, and S. Spigarelli, "Wear resistance investigation of titanium nitride-based coatings," *Ceramics International*, vol. 41, no. 9, pp. 10349–10379, May 2015, doi: 10.1016/j.ceramint.2015.04.152.

[21] K. Pondicherry, D. Rajaraman, T. Galle, S. Hertelé, D. Fauconnier, and P. De Baets, "Optimization and validation of a Load-Controlled Numerical model for single asperity scratch," *Tribology Letters*, vol. 68, no. 1, Feb. 2020, doi: 10.1007/s11249-020-1283-3.

[22] P. Wechsuwanmanee *et al.*, "Finite element model in abrasion Analysis for Single-Asperity Scratch Test," in *Lecture notes in mechanical engineering*, 2018, pp. 768–779, doi: 10.1007/978-981-13-0411-8_68.

[23] M. A. Masen, M. B. De Rooij, and D. J. Schipper, "Micro-contact based modelling of abrasive wear," *Wear*, vol. 258, no. 1–4, pp. 339–348, Oct. 2004, doi: 10.1016/j.wear.2004.09.009.

[24] T.-B. Mac, T.-T. Luyen, and D.-T. Nguyen, "A Study for Improved Prediction of the Cutting Force and Chip Shrinkage Coefficient during the SKD11 Alloy Steel Milling," *Machines*, vol. 10, no. 4, p. 229, Mar. 2022, doi: 10.3390/machines10040229.

[25] G. R. Johnson and W. H. Cook, "Fracture characteristics of three metals subjected to various strains, strain rates, temperatures and pressures," *Engineering Fracture Mechanics*, vol. 21, no. 1, pp. 31–48, Jan. 1985, doi: 10.1016/0013-7944(85)90052-9.

[26] K. Bobzin *et al.*, "Investigation on plastic behavior of HPPMS CrN, AlN and CrN/AlN-multilayer coatings using finite element simulation and nanoindentation," *Surface and Coatings Technology*, vol. 284, pp. 310–317, Aug. 2015, doi: 10.1016/j.surfcoat.2015.07.081.

[27] Q. Cai, X. Bai, Y. Zeng, and X. Zhang, "The mechanical properties and damage mechanism of TiAlN/TiZrHfNb coatings subjected to dynamic cyclic nano-impact," *Surface and Coatings Technology*, vol. 512, p. 132283, May 2025, doi: 10.1016/j.surfcoat.2025.132283.

[28] B. D. Beake, J. Roberts, Y. Zhu, and T. W. Liskiewicz, "Simulating erosion tests with statistically distributed micro-scale impact: A study on PVD TiAlN and AlCrN coatings," *Wear*, vol. 570, p. 205911, Feb. 2025, doi: 10.1016/j.wear.2025.205911.

[29] M. Kopernik, A. Milenin, R. Major, and J. M. Lackner, "Identification of material model of TiN using numerical simulation of nanoindentation test," *Materials Science and Technology*, vol. 27, no. 3, pp. 604–616, Jul. 2010, doi: 10.1179/026708310x12756557336193.

[30] V. Bonu, S. Kumar, P. N. Sooraj, and H. C. Barshilia, "A novel solid particle erosion resistant Ti/TiN multilayer coating with additional energy absorbing nano-porous metal layers: Validation by FEM analysis," *Materials & Design*, vol. 198, p. 109389, Dec. 2020, doi: 10.1016/j.matdes.2020.109389.

[31] Z. Yuan *et al.*, "Damage evolution behavior of TiN/Ti multilayer coatings under high-speed impact conditions," *Surface and Coatings Technology*, vol. 426, p. 127807, Oct. 2021, doi: 10.1016/j.surfcoat.2021.127807.

[32] W. Liu *et al.*, "Toughening mechanism analysis of TiN/TiSiN coatings with modulation period gradient structure," *Journal of Materials Research and Technology*, vol. 35, pp. 4109–4121, Feb. 2025, doi: 10.1016/j.jmrt.2025.02.098.

[33] Y. B. Ammar, K. Aouadi, A. Besnard, A. Montagne, C. Nouveau, and F. Bouchoucha, "Exploring the effect of layer thickness on the elastoplastic properties of the constituent materials of CrN/CrAlN multilayer coatings: a nanoindentation and finite element-based investigation," *Thin Solid Films*, vol. 808, p. 140581, Nov. 2024, doi: 10.1016/j.tsf.2024.140581.

[34] N. Fereshteh-Saniee, H. Elmkhah, M. Nouri, and M. Meghdari, "An investigating of how mechanical properties impact the erosion resistance of CrN, CrTiN, and CrTiSiN PVD coatings," *Results in Surfaces and Interfaces*, vol. 18, p. 100422, Jan. 2025, doi: 10.1016/j.rsurfi.2025.100422.

[35] L. K. Sharma, N. K. Sharma, A. K. Dash, and A. S. Rana, "Finite element analysis of TiN coated thin film," *Materials Today Proceedings*, vol. 113, pp. 274–277, Sep. 2023, doi: 10.1016/j.matpr.2023.09.149.

[36] K. Zhuang, K. Zhu, X. Wei, C. Hu, Z. Liu, and Z. Gao, "A dual-stage wear rate model based on wear mechanisms analysis during cutting Inconel 718 with TiAlN coated tools," *Journal of Manufacturing Processes*, vol. 126, pp. 24–34, Jul. 2024, doi: 10.1016/j.jmapro.2024.07.089.

[37] C. Wang, F. Ding, D. Tang, L. Zheng, S. Li, and Y. Xie, "Modeling and simulation of the high-speed milling of hardened steel SKD11 (62 HRC) based on SHPB technology," *International Journal of Machine Tools and Manufacture*, vol. 108, pp. 13–26, Jun. 2016, doi: 10.1016/j.ijmachtools.2016.05.005.

[38] J. M. Challen and P. L. B. Oxley, "An explanation of the different regimes of friction and wear using asperity deformation models," *Wear*, vol. 53, no. 2, pp. 229–243, Apr. 1979, doi: 10.1016/0043-1648(79)90080-2.

[39] K. Hokkirigawa and K. Kato, "An experimental and theoretical investigation of ploughing, cutting and wedge formation during abrasive wear," *Tribology International*, vol. 21, no. 1, pp. 51–57, Feb. 1988, doi: 10.1016/0301-679x(88)90128-4.

[40] K. Kato and K. Adachi, "Wear mechanisms," in *Modern tribology handbook: volume one: principles of tribology*, CRC press, 2000, pp. 273–300.

[41] K. Hokkirigawa, K. Kato, and Z. Z. Li, "The effect of hardness on the transition of the abrasive wear mechanism of steels," *Wear*, vol. 123, no. 2, pp. 241–251, Apr. 1988, doi: 10.1016/0043-1648(88)90102-0.

[42] Ş. Danışman, D. Odabaş, and M. Teber, "The effect of TIN, TIALN, TICN thin films obtained by reactive magnetron sputtering method on the wear behavior of TI6AL4V alloy: a comparative study," *Coatings*, vol. 12, no. 9, p. 1238, Aug. 2022, doi: 10.3390/coatings12091238.

[43] B. A. Rao, M. Tak, R. N. Rao, and R. Bathe, "Investigations on the tribological performance of Inconel-625 and Tungsten carbide tribo-pairs in dry sliding wear at elevated temperatures," *Materials Letters*, vol. 389, p. 138393, Mar. 2025, doi: 10.1016/j.matlet.2025.138393.

[44] K. Kusumoto *et al.*, "High-temperature erosive wear characteristics and bonding requirements of hard carbides cast-in insertion multi-component white cast iron," *Wear*, vol. 476, p. 203672, Feb. 2021, doi: 10.1016/j.wear.2021.203672.

[45] G. O. Barrionuevo, H. Calvopiña, A. Debut, and C. Pérez-Salinas, "Experimental and numerical investigation of sliding wear of heat-treated 316L stainless steel additively manufactured," *Journal of Materials Research and Technology*, vol. 33, pp. 2692–2703, Oct. 2024, doi: 10.1016/j.jmrt.2024.09.263.